KI REPORTS
KIReports.org
TRANSLATIONAL RESEARCH

The Role of Mitochondrial AKT1 Signaling in Renal Tubular Injury of Metabolic Syndrome

Hugo Y.-H. Lin[1,2,3], I-Ya Chen[4], Tzu-Ming Wang[5], Chia-Hung Yen[6], Yumay Chen[7], Yen-Hua Chen[8], Dao-Fu Dai[9], Jee-Fu Huang[10], Yi-Wen Chiu[1,12] and Ming-Yu Yang[4,11,12]

[1]Division of Nephrology, Department of Internal Medicine, Kaohsiung Medical University Hospital, Kaohsiung, Taiwan; [2]Department of Medicine, Kaohsiung Medical University, Kaohsiung, Taiwan; [3]Graduate Institute of Medicine, College of Medicine, Kaohsiung Medical University, Kaohsiung, Taiwan; [4]Graduate Institute of Clinical Medical Sciences, College of Medicine, Chang Gung University, Taoyuan, Taiwan; [5]Department of Medical Research, China Medical University Hospital, Taichung, Taiwan; [6]Graduate Institute of Natural Product, College of Pharmacy, Kaohsiung Medical University, Kaohsiung, Taiwan; [7]School of Medicine, University of California, Irvine, California, USA; [8]School of Medicine, Doctoral Program of Clinical and Experimental Medicine, Institute of Biomedical Sciences, College of Medicine, National Sun Yat-Sen University, Kaohsiung, Taiwan; [9]Department of Pathology, Johns Hopkins University School of Medicine, Baltimore, Maryland, USA; [10]Hepatobiliary Division, Department of Internal Medicine, Kaohsiung Medical University Hospital, Kaohsiung Medical University, Kaohsiung, Taiwan; and [11]Department of Otolaryngology, Kaohsiung Chang Gung Memorial Hospital and Chang Gung University College of Medicine, Kaohsiung, Taiwan

Introduction: Metabolic syndrome (MetS) is increasingly recognized as a contributor to kidney disease, yet the underlying mechanisms remain poorly defined. Recent studies suggest a pivotal role for mitochondrial dysfunction in renal injury. We hypothesized that mitochondrial AKT1 signaling in renal tubules plays a critical role in MetS-related kidney injuries.

Methods: MetS was induced in a 8-week-old C57BL/6 male mice using a high-fat diet (HFD) for 4 months compared with controls on a standard chow diet. Additional experiments were conducted in DB/DB diabetic mice and their controls (WT and DB/WT) to validate findings. Renal metabolic parameters, mitochondrial AKT1 signaling, and markers of kidney injury were assessed.

Results: MetS mice exhibited significant weight gain, altered glucose handling, and decreased energy expenditure. Although kidney size and basic renal function (blood urea nitrogen [BUN], creatinine) were unchanged, markers of renal damage, including proteinuria ($P = 0.0002$) and KIM-1 ($P < 0.0001$) were elevated. Histological analyses showed increased tubular injury ($P < 0.0001$) and glomerulosclerosis ($P = 0.0004$). Transmission electron microscopy revealed aberrant mitochondria ($P < 0.001$), with reduced cristae length ($P = 0.012$) and numbers ($P < 0.001$). Immunohistochemistry, immunofluorescence, and Western blot analysis confirmed increased phosphorylated AKT1 (pAKT1) in the mitochondria of renal tubules ($P = 0.0474$), findings corroborated in DB/DB mice. This translocation of pAKT1 into mitochondria correlated with decreased cell viability upon inhibition of heat shock protein 90, indicating a dependency on mitochondrial AKT1 for cell survival.

Conclusion: These findings underscore the mechanistic link between mitochondrial AKT1 signaling and renal tubular injury in MetS. Targeting mitochondrial dysfunction may offer new avenues for preventing and treating kidney diseases in patients with MetS.

Kidney Int Rep (2025) **10,** 906–920; https://doi.org/10.1016/j.ekir.2024.12.021
KEYWORDS: AKT1 signaling; kidney disease; metabolic syndrome; mitochondrial dysfunction; renal tubular injury

Correspondence: Ming-Yu Yang, Graduate Institute of Clinical Medical Sciences, College of Medicine, Chang Gung University, No. 259, Wenhua 1st Road, Guishan District, Taoyuan City, Taiwan. E-mail: yangmy@mail.cgu.edu.tw; or Yi-Wen Chiu,Division of Nephrology, Kaohsiung Medical University Hospital, 100, Shih-Chuan 1st Road, Kaohsiung, Taiwan. E-mail: k81069@kmu.edu.tw

[12]Y-WC and M-YY contributed equally

Received 29 July 2024; revised 2 December 2024; accepted 10 December 2024; published online 24 December 2024

MetS comprises a collection of metabolic issues, such as central obesity, dyslipidemia, hypertension, and insulin resistance, which together elevate the risk of cardiovascular diseases, type 2 diabetes mellitus, and kidney diseases.[1] It is an increasingly severe public health issue and clinical challenge worldwide.[2] Among these, the association between MetS and kidney diseases has garnered significant interest, with studies suggesting a link between MetS and the development

and progression of kidney injury.[3–7] However, the precise mechanisms underlying this association remain unclear.

Mitochondrial dysfunction is emerging as a critical player in the pathogenesis of various metabolic disorders, including MetS.[8] Mitochondria play crucial roles in cellular energy metabolism, and their dysfunction has been implicated in insulin resistance, dyslipidemia, and oxidative stress, all of which are hallmark features of MetS.[9] Recent evidence suggests that mitochondrial dysfunction in renal tubular cells may contribute to the development of kidney injuries in the context of MetS.[10,11]

The serine/threonine kinase AKT1, a key regulator of cellular metabolism and survival, has been shown to modulate mitochondrial function.[12] AKT1 signaling is known to regulate mitochondrial biogenesis, dynamics, and function, and dysregulation of this pathway has been implicated in various metabolic disorders.[13,14] In our previous research, we found that AKT1 is activated and translocated into mitochondria during ischemia and reperfusion renal injuries.[15] However, the role of AKT1 signaling in mitochondrial dysfunction and kidney injury in the setting of MetS has not been thoroughly investigated. Elucidating this signaling pathway is crucial and may enable the identification of novel therapeutic targets, potentially mitigating kidney injury in MetS.

Considering these observations, we hypothesized that renal tubular mitochondrial AKT1 signaling plays a mechanistic role in the pathogenesis of MetS-related kidney injuries. To test this hypothesis, we utilized a murine model of MetS induced by HFD, and investigated the impact of MetS on renal tubular mitochondrial AKT1 signaling and kidney injury.

METHODS

Materials

Phospho-AKT1 (T308) antibodies (AP0304) were purchased from Abclonal (China). VDAC polyclonal antibody was purchased from Elab (E-AB-52417, Houston, TX). ATP1F1: Abcam ab110277 was from Abcam. Secondary antibody Alexa Fluor 594 (A21203) and secondary antibody Alexa Fluor488 (A21206) were purchased from Invitrogen (Carlsbad, CA). KIM-1 (#AF1817) antibodies were purchased from R&D Systems (Minneapolis, MN). The EnzyChrom creatinine assay kit (#E2CT-100), EnzyChrom urea assay kit (#E2CT-100), QuantiChrom BCG albumin assay kit (#DIAG-250) were purchased from BioAssay Systems (Hayward, CA). The Ultra-Sensitive Mouse Insulin enzyme-linked immunosorbent assay kit was purchased from CiteAb (Bath, UK). Chemicals and reagents were from Sigma Aldrich (St Louis, MO).

In Vivo Model of MetS

All animal work was performed in an accredited facility accredited by the Association for Assessment and Accreditation of Laboratory Animal Care International. The Institutional Animal Care and Use Committee approved the experimental protocol at Kaohsiung Medical University and complied with the National Institutes of Health guidelines. Eight-week-old C57BL/6J mice (Jackson Laboratory, Bar Harbor, ME) were used for the study. The HFD (Research Diet Inc.: DIO [HFD] 45 kcal% fat D12451) (21.2% fat, 49.1% carbohydrate [34.1% sucrose +15% cornstarch], 17.3% protein, 5.0% fiber, 3.5% minerals, 0.4% $CaCO_3$, 1% vitamin mix, 0.004% antioxidants, and 0.2% cholesterol) was utilized. Mice were kept at ambient temperature (30 °C–32 °C). Control mice were subjected to the same procedure (standard chow diet).

Analysis of Metabolic Parameters

During week 16, individual mice's energy intake and metabolic activity were measured using TSE PhenoMaster cages (TSE systems, Bad Homburg, Germany). The TSE PhenoMaster cages comprised an open-circuit indirect calorimetry system with gas sensing units to measure oxygen consumption (ml/h/kg) (VO2) and CO_2 production (ml/h/kg) (VCO2). The cages also contained high-precision sensor-associated-feeding baskets to accurately measure food intake, with a meal defined as intake over 0.01 g. A multidimensional infrared beam system allowed the measurement of locomotor activity, defined as the total number of infrared beam breaks in the X and Y axes. Mice were singly housed in TSE PhenoMaster cages for 3 days, with data collected during the final 24 hours following a 2-day acclimatization to the new cage environment. The acclimatization period was established based on the data from our previous study.[16] Heat production (kcal/h/kg) in individual mice was calculated using the Weir equation (3.9416 VO2 + 1.1066 VCO2),[17] and this was converted to kJ/h/kg using 1 kcal = 4.184 kJ. VCO2/VO2 was calculated as the respiratory exchange ratio. Energy intake was calculated from food intake measurements using the energy content of the diets supplied by the manufacturer.

Blood Glucose, Intraperitoneal Glucose Tolerance Test (IPGTT)

Blood glucose levels were measured by using glucose meter (Optium Xceed XCN 289-2337, Abbott, Chicago, IL). For IPGTT, blood glucose was measured immediately before and at 5, 15, 30, 60, 90, and 120 minutes

after an intraperitoneal glucose (2 g/kg in 0.9% NaCl) injection.

Serum BUN and Creatinine

Blood was collected from the retro-orbital plexus under anesthesia for serum BUN and creatinine levels. Serum was obtained by centrifugation at 10,000g for 30 minutes at room temperature. BUN or creatinine levels were determined with colorimetric assay kits according to the manufacturer's instructions (BioAssay Systems, Hayward, CA) and a plate reader (Biotek Synergy HT, Winooski, VT).

Histology and Immunohistochemistry

Kidney samples were fixed in 10% formalin for 24 hours, dehydrated, and embedded in paraffin. Paraffin-embedded kidney blocks were sectioned at 4 μm thickness. Hematoxylin and eosin staining were performed to assess general morphology and renal structure injury. Renal damage in proximal tubules from the cortex area and outer stripe of the kidney's outer medulla was evaluated with a semiquantitative analysis of histologically damaged areas as previously described.[18] The Jablonski grading scale (0–4) was used to assess the proximal tubules.[19] A score of 1 indicates minimal damage, which may be reversible or indicate early-stage injury. Scores of 2 or 3 reflect moderate to significant damage, potentially requiring medical intervention and closer monitoring. A score of 4 signifies severe damage, likely associated with considerable functional impairment of the kidneys and possibly irreversible injury. To visualize p-AKT expression by immunohistochemistry staining, sections were incubated with p-AKT1 antibody and biotinylated α-rabbit secondary antibody (Vector Lab) for 45 minutes at room temperature. At least 20 microscopic fields were randomly selected from each tissue section, and ImageJ was used to assess the percentage of positively stained tubules for quantitative analysis. The investigators who scored the histology images were blinded to the samples.

Immunofluorescence

Frozen OCT-embedded kidney sections were sliced for 5μm and excess OCT removed with phosphate-buffered saline (PBS) wash for 10 minutes. After washing, the tissue sections were circled with a liquid Blocker Super Pap Pen before blocking with 5% bovine serum albumin in PBS for 1 hour at room temperature. Slides were washed by PBST (PBS with 0.2% Triton X-100) before applying Phospho-AKT1 antibody (400-folds diluted by antibody diluent reagent solution, Invitrogen, 003218) and incubated overnight in a humified chamber at 4 °C. With PBST, slides applied ATP1F1 antibody (100-fold diluted by antibody diluent reagent solution) and incubated overnight in a humified chamber at 4 °C. After being extended and washed with PBS, fluorescent-conjugated secondary antibodies were applied and placed in the humified chamber for 1 hour at room temperature. After washing with PBST, slides were stained for 5 minutes by DAPI (1000-fold diluted by PBS, Thermo Fisher, 62248) and then mounted (ProLong Diamond Antifade Mountant, Invitrogen, P36961) for analysis with laser confocal microscopy (FV10i; Olympus, Tokyo, Japan).

Mitochondria Preparation

Renal cortical and outer medulla tissues were isolated from the kidney, minced, washed with ice-cold PBS 3 times, and suspended in a mitochondria isolation buffer (20 mM HEPES-KOH, pH 7.2, 10 mM KCl, 1.5 mM $MgCl_2$, 1.0 mM EDTA, 1.0 mM EGTA, 1.0 mm dithiothreitol, 2 phenylmethylsulfonyl fluoride, 20 mM NaF, 2 mM Na_3VO_4, and 250 mM sucrose. The samples were incubated on ice for 30 minutes and homogenized with 20 strokes of loose pestle and 50 strokes of tight pestle in a Dounce homogenizer. The nuclei and cell debris were removed by centrifugation at 1000g for 15 minutes at 4 °C. The supernatants were centrifuged at 10,000g for 4 °C for 30 minutes, and the resulting mitochondrial fractions were resuspended with mitochondria isolation buffer. The supernatants were further centrifuged at 100,000g at 4 °C for 1 hour. The cytosolic and mitochondrial fractions were stored at −80 °C if not immediately used for analysis.

Western Blots Analysis

The mitochondrial fractions were dissolved in a 2% lauryl maltoside solution supplemented with 10% Sigma FAST protease inhibitor (Sigma-Aldrich, S8820). Protein concentrations were determined by the BCA method. Equal amounts of proteins from each sample were resolved with 10% SDS-polyacrylamide gel and then transferred onto polyvinylidene difluoride membranes. The membranes were blocked with 5% fat-free milk or 5% bovine serum albumin for 1 hour at room temperature before incubation with primary antibodies overnight at 4 °C. After being washed 3 times with TBS-T (20mM Tris–HCl, pH 7.5, 0.5 mm NaCl, and 0.1% Tween 20), the membranes were incubated with horseradish peroxidase-conjugated secondary antibodies (1:2000 dilution in 5% fat-free milk or 5% bovine serum albumin) for 1 hour at room temperature. After 3 washes, the membranes were developed with West Pico Chemiluminescent Substrate (Thermo Scientific, Pittsburgh, PA), and the images were acquired with a Luminescence image system and analyzed with ImageJ.

In Vitro Model of MetS-Related Kidney Injuries

HK-2 cells (human kidney proximal tubular cells) were purchased from the American Type Culture Collection (Manassas, VA). HK-2 cells were cultured in commercial keratinocyte medium containing 10% fetal bovine serum (FBS; HyClone), 2 mM glutamine, 100 U/ml penicillin, and 100 mg/ml streptomycin in a humidified atmosphere with 5% CO_2 at 37 °C. In preparation for treatment of palmitic acid (T2908, TargetMol, Boston, MA, USA), cells were seeded in clear-bottom 96-well plates (Greiner, Frienckenhausen, Germany) at a density of 1x 105. Serially diluted concentrations of palmitic acid were prepared in HK-2 media. All treatments were added to appropriate wells for the intended exposure duration and kept at 37 °C in a humidified incubator with 5% CO_2 before performing experiments. For the *in vitro* study, HK-2 cells were induced with palmitic acid at 50 μM, 100μM, and 200μM for 48 hours separately. PU-H71 (T6960, TargetMol, Boston, MA) and Alvespimycin hydrochloride (T6297, TargetMol, Boston, MA) were added separately. The Cell Counting Kit-8 assay (C0005, TargetMol, Boston, MA, USA) was used to measure cell viability of HK2 cells.

Transmission Electron Microscopy

The kidney tissues from mice were immersed into 3% glutaraldehyde + 2% paraformaldehyde in 0.1 M cacodylate buffer (pH 7.4), protected from light in a refrigerator at 4 °C. Moreover, the samples were replaced with 0.1 M cacodylate buffer (pH 7.4) for 10 minutes 3 times and stored in a refrigerator at 4 °C. Then, they were replaced with 1% OsO4 in 0.1 M cacodylate buffer for 1 hour and stored in a refrigerator at 4 °C to avoid light. We used 0.1 M cacodylate buffer (pH 7.4) for 10 minutes once in total and overnight in a refrigerator at 4 °C. Moreover, we replaced it with secondary water for 10 minutes twice at room temperature, 2% uranyl acetate (in H_2O) for 1 hour, protection from light at room temperature, and secondary water for 10 minutes 3 times at room temperature. The tissue was dehydrated with 30%, 50%, 70%, 95%, and 100% alcohol for 10 minutes in a refrigerator at 4 °C. Then, the tissue was replaced with 100% propylene oxide 10 minutes 2 times at room temperature. Furthermore, the tissue was infiltrated with propylene oxide: Epon = 3:1 at room temperature overnight, propylene oxide: Epon = 1:1 at room temperature for 7 hours, and propylene oxide: Epon = 1:3 at room temperature overnight. The tissue was then embedded: 100% Epon and specimen were put into the embedding plate, and then the tissue was put into a vacuum for air extraction overnight. The tissues were put into the oven and set 3 times at temperatures 35 °C for 6 hours, 45 °C for 6 hours, 60 °C for 24 hours, and cut into thick sections: thickness of 500 nm. The sections were stained. Thick sections: 0.5% Toluidine blue for 1 minute, then the location where thin sections needed to be cut were selected. Moreover, the thick section was cut of ultrathin slices: thickness 80 ± 5 nm. The ultrathin section was stained with 4% uranyl acetate in H_2O for 2 hours and 4% lead citrate and colored for 8 minutes. They were observed and photos were taken on the Hitachi HT7800 transmission electron microscope.

Statistical Analysis

Data were presented as mean ± SD unless noted otherwise. Statistical data were analyzed with GraphPad Prism 7 software (GraphPad Software, San Diego, CA), with analysis of variance when indicated. The western blot region of interest was quantified by using ImageJ, normalized with the region of interest value of loading control, and analyzed with *t*-test. The statistical significance level was set at $P < 0.05$. Survival analysis was analyzed with the Kaplan–Meier estimator.

RESULTS

HFD-Induced MetS in Mice

The first goal was to investigate whether the HFD could induce MetS *in vivo*. We successfully established a MetS mouse model by feeding HFD (21.2% fat, 49.1% carbohydrate [34.1% sucrose + 15% cornstarch], 17.3% protein, 5.0% fiber, 3.5% minerals, 0.4% $CaCO_3$, 1% vitamin mix, 0.004% antioxidants, and 0.2% cholesterol) to C57BL6 male mice for 16 weeks. Before treatment, there were no differences in baseline body weight and fasting blood glucose between the HFD and control groups (Figure 1a, Supplementary Figure S1A). Upon HFD, the mice had a progressive body weight gain (Figure 1a), which was highly significant at 16 weeks ($P < 0.0001$) (Figure 1b). To study the glucose metabolism in HFD, we analyzed fasting plasma glucose, intraperitoneal glucose, and insulin. The fasting plasma glucose ($P < 0.0001$) was significantly higher (in the diabetic range) in the HFD group compared with the standard chow group (Figure 1c). In the IPGTT, it was observed that mice fed with HFD had significantly higher glucose levels from 15 to 120 minutes compared with those receiving chow diet ($P = 0.022$) (Figure 1d). The slope of the IPGTT curve in the HFD group was steeper than that of the standard chow group, and the area under the curve value was higher ($P < 0.0001$) (Figure 1e). Fasting insulin levels were significantly higher after 16 weeks of HFD ($P < 0.0001$, Figure 1f). Consequently, mice in the HFD group exhibited elevated homeostasis model assessment of insulin resistance values ($P < 0.0001$, Figure 1g). These

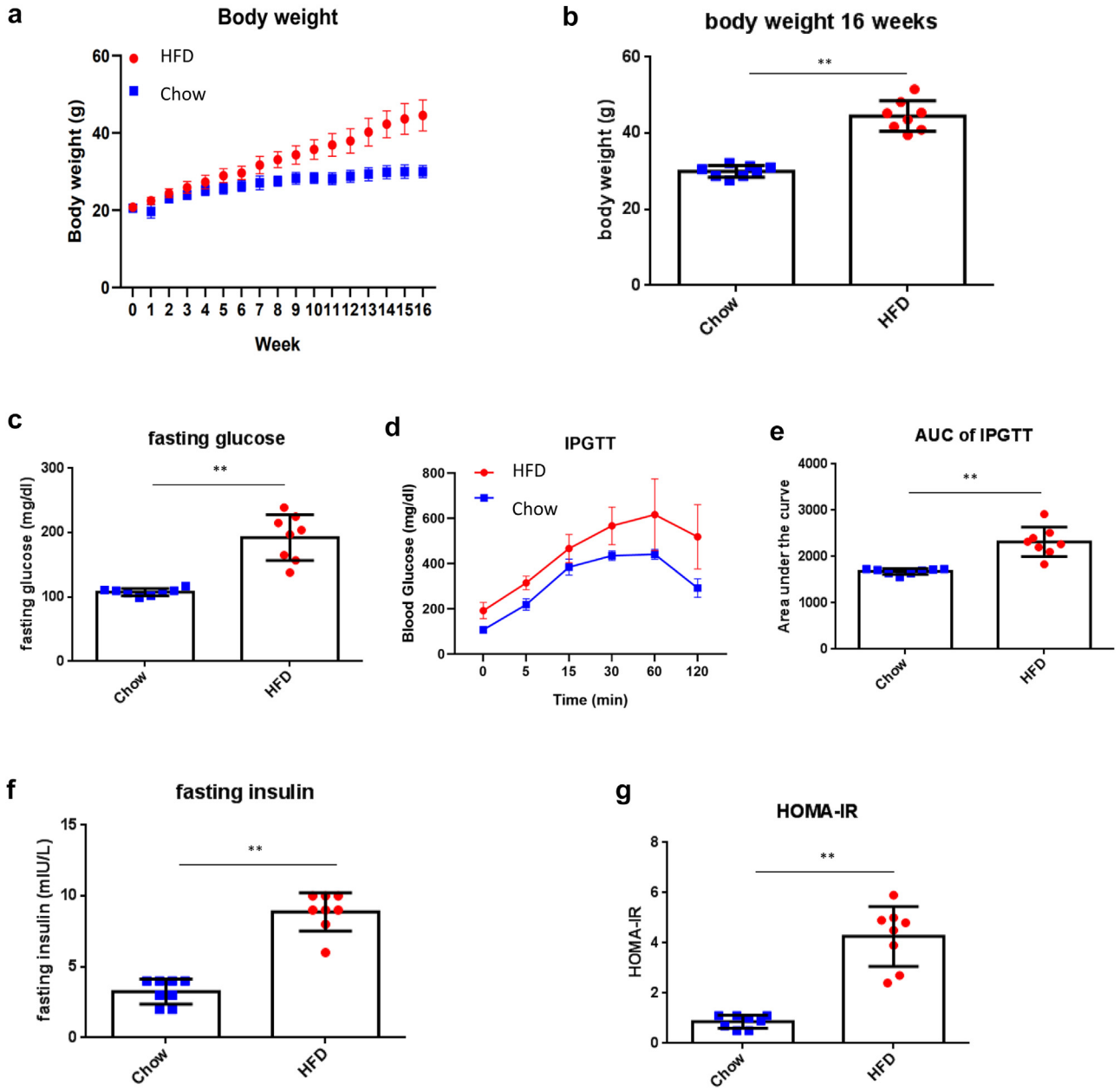

Figure 1. High-fat diet induced metabolic syndrome. After feeding 16-week HFD, body weight and plasma were measured. (a) Body weights changes from 0 to 16 weeks of feeding. (b) Body weight was significantly higher in the HFD group compared with the standard chow diet group in week 16 ($P < 0.001$). (c) The fasting blood glucose levels were significantly higher in the HFD group compared with the standard chow diet group ($P < 0001$). (d) In the IPGTT, the glucose levels were significantly elevated ($P = 0.022$). The shape of the HFD group curve was dissimilar to that of the control group. (e) The AUC level of IPGTT was higher ($P = 0.015$). (f) Dapgliflozin lowered the fasting insulin levels ($P < 0.001$). (g) Insulin resistance, as assessed by HOMA-IR, was significantly elevated ($P < 0.001$). Data are presented as mean ± SD. HFD ($n = 8$), standard chow diet ($n = 8$) as control. *$P < 0.05$, **$P < 0.01$ or ***$P < 0.001$ versus control group. AUC, area under the curve; HFD, high-fat diet; HOMA-IR, homeostasis model assessment of insulin resistance; IPGTT, intraperitoneal glucose tolerance test.

results collectively indicated that HFD induced MetS and glucose intolerance.

MetS Decreased Energy Expenditure

To investigate the overall metabolism in MetS, we employed the metabolic cage system (TSE System PhenoMaster). Mice were individually housed and monitored to track oxygen consumption (VO2) and carbon dioxide production (VCO2). Although cumulative food and water intake over 16 weeks did not differ significantly between the HFD group and the standard chow diet group (4623 cal/mouse/d vs. 5038 cal/mouse/d, and 1.466 ml/mouse/d vs. 0.789 ml/mouse/d, respectively) (Figure 2b and c), there was a significant decrease in fluid intake during the dark phase ($P = 0.0379$). The HFD group exhibited significantly reduced VO2 ($P < 0.0001$), VCO2 ($P < 0.0001$), respiratory exchange ratio ($P < 0.0001$), and heat production ($P < 0.0001$)

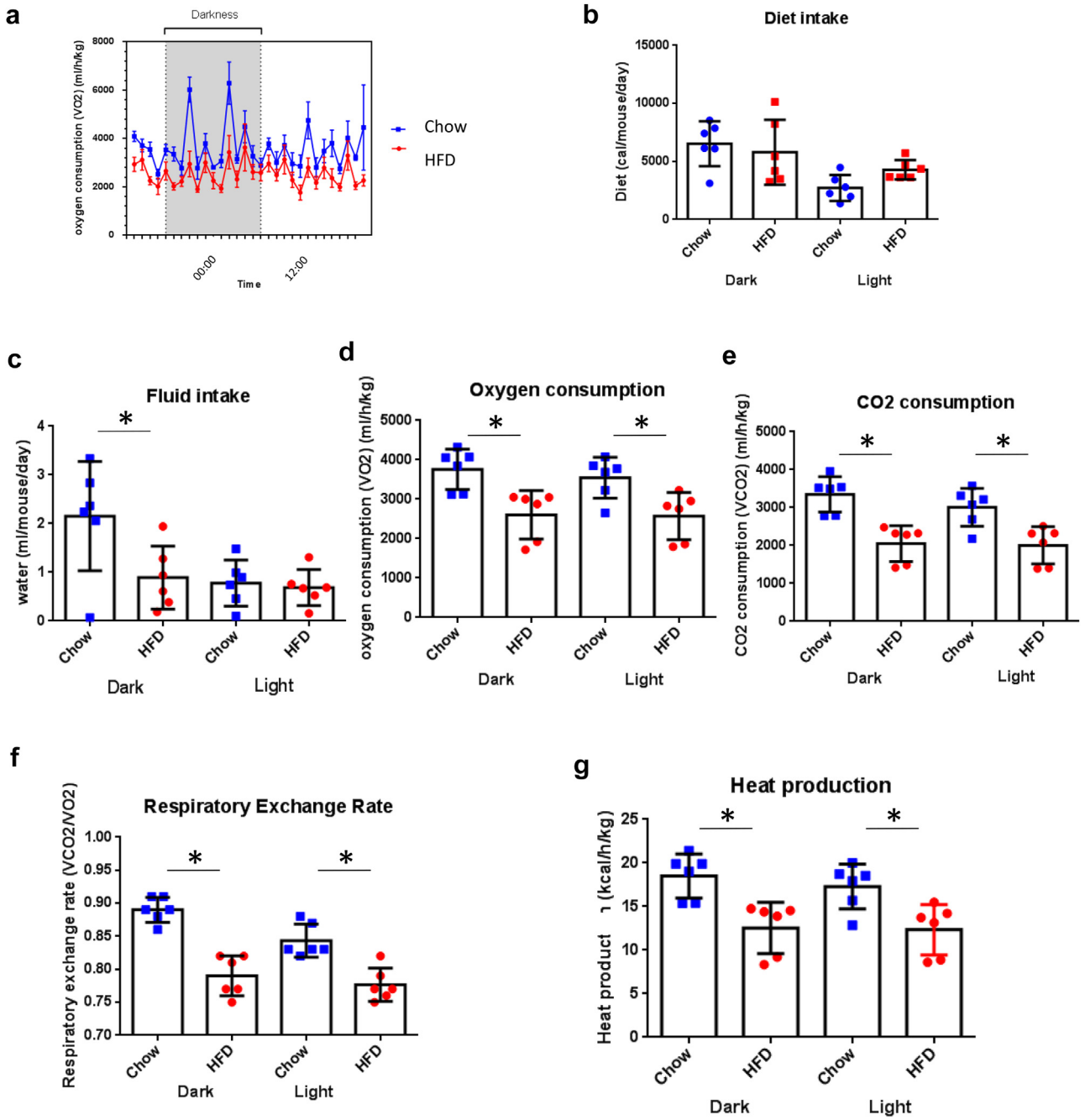

Figure 2. Metabolic syndrome suppressed food intake and energy expenditure. Metabolic cage analysis was performed on mice after 4 months of HFD. (a) Kinetic data for oxygen consumption ($n = 6$ in each group) are shown as the mean for each time point and summarized as means for light and dark periods. (b) There were no significant differences in diet intake between the HFD and control group. (c) HFD mice had a lower fluid intake in the dark. (d–g) There were significantly lower oxygen consumption, CO_2 consumption, respiratory exchange rate, and heat production in the HFD group ($P < 0.05$). HFD, high-fat diet.

compared with the standard chow diet group (Figure 2d–g). These measurements were corroborated by data from the TSE PhenoMaster cages (Figure 2a).

Renal Injuries Induced by MetS

To gain further insight into the renal manifestations of MetS, we conducted plasma and urine biochemical analyses. Before the HFD, there were no significant differences in renal structure or serum creatinine levels (Supplementary Figure S1B–D). After 16 weeks, despite the absence of significant differences in plasma creatinine and BUN levels between HFD mice and the control group (Figure 3a and b), HFD mice exhibited significantly higher levels of proteinuria ($P = 0.0002$) and urinary KIM-1 ($P < 0.0001$) (Figure 3c and d). These findings confirm the induction of renal injuries by

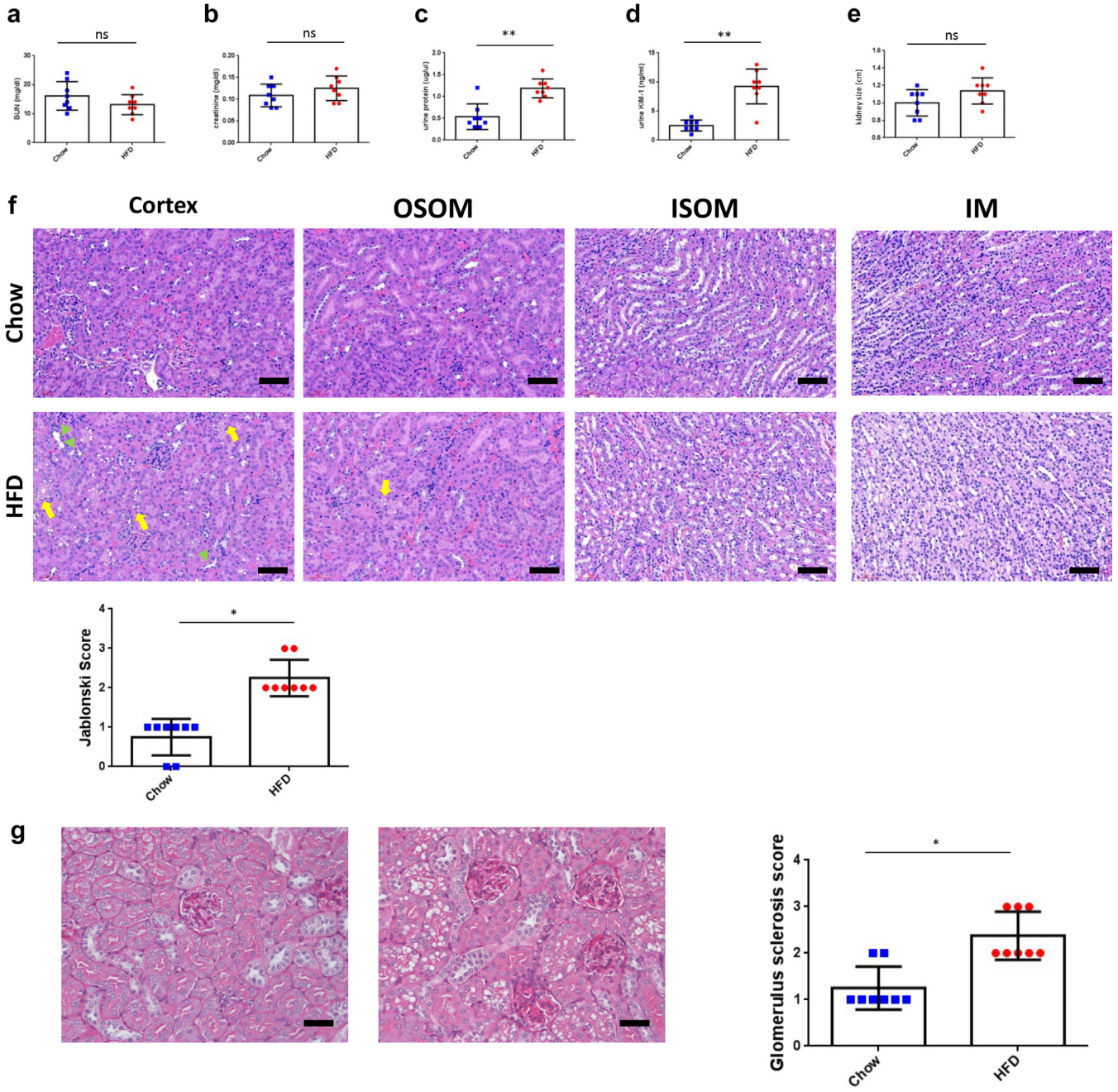

Figure 3. Metabolic syndrome induced renal injuries. (a and b) Serial measurements showed no significant BUN and creatinine (Cr) changes after 4 months of HFD. (c–d) Significantly higher proteinuria ($P = 0.0002$) and urinary KIM-1 ($P < 0.0001$) levels were observed in the HFD mice. (e) There were no significant differences in kidney size between mice fed HFD and those on a normal chow diet. (f) Renal tissue sections were hematoxylin and eosin– stained to estimate renal injuries. The upper panel shows representative microscopic images of standard chow diet group, the lower panel is a summary of the results from the HFD group. Jablonski scores for renal tubular injuries were elevated ($P = 0.0031$), and there were more vacuolized renal tubules ($P < 0.0001$). (g) In addition, the glomerulosclerosis index was significantly higher ($P = 0.0004$) with PAS staining. Glomerulosclerosis was analyzed. The glomerulus is graded as follows: 0 (no lesions), 1 (lesions in up to 25% of glomeruli), 2 (lesions in 25%–50% of glomeruli), or 3 (lesions in $>$ 50% of glomeruli). At least 50 glomeruli were scored for each mouse (8 mice in each group); the results are summarized in graph h. (***$P < 0.001$). BUN, blood urea nitrogen. PAS, periodic acid–Schiff.

MetS. To examine changes in renal structure, we analyzed kidney size and histology. There were no significant differences in kidney size between the HFD group and the standard chow diet group (Figure 3e). However, HE staining of renal sections revealed aggravated renal injuries in HFD mice (Figure 3f). Jablonski scores for renal tubular injuries were elevated (Figure 3f, $P = 0.0031$), and there were more

vacuolized renal tubules ($P < 0.0001$). In addition, the glomerulosclerosis index was significantly higher ($P = 0.0004$) among periodic acid–Schiff staining (Figure 3g).

MetS Altered the Mitochondrial Ultrastructure of Renal Tubular Cells

Considering these observations of renal tubular injuries, we aimed to investigate the underlying cellular mechanisms. Renal tubular cells are highly metabolic and heavily reliant on mitochondrial function. Consequently, MetS-induced renal tubular injuries may be associated with alterations in tubular mitochondrial structure and function. To test this hypothesis, we conducted a series of experiments to assess the mitochondrial ultrastructure in these cells. Morphometric analysis of renal tubular cells in HFD mice was performed using transmission electron microscopy. Mice fed an HFD exhibited an increased number of atypical mitochondria in renal tubular cells compared with the control group (Figure 4a). Morphometric analysis revealed a significantly higher aberrant mitochondrial area ratio (28.13 ± 2.39% mitochondria per field in HFD vs. 4.00 ± 0.42% in the standard chow diet group) ($P < 0.0001$) (Figure 4b). Furthermore, a significant decrease in the total cristae length of the mitochondrial area was observed in the HFD group compared with the standard chow diet group (3.46 ± 0.2 $\mu m/\mu m^2$ vs. 5.21 ± 0.38 $\mu m/\mu m^2$) ($P = 0.0012$) (Figure 4c). The cristae number per mitochondrial area was also significantly reduced (20.00 ± 1.78 per mitochondrial area in HFD vs. 37.13 ± 2.17 in the standard chow diet group) ($P < 0.0001$) (Figure 4d). These findings suggest that MetS induces mitochondrial deformation and cristae disorganization.

Activation and Translocation of AKT to Mitochondria in Renal Tubules upon MetS

A further goal was to investigate whether AKT can be translocated and activated in renal tubules upon MetS. The renal cortex, enriched with renal tubules, was isolated, and the mitochondria were subfractionated by gradient centrifugation. Upon MetS, the abundance of pAKT1 increased in mitochondria, suggesting the translocation of AKT1 into mitochondria (Figure 5a).There was a significant increase of mitochondrial pAKT1 in MetS ($P = 0.0474$) compared with the control group. Activation of AKT1 in renal tubules after MetS was confirmed with immunohistochemistry staining (Figure 5b). There was only minimal pAKT1 staining in the renal tubule of the standard chow diet group, whereas pAKT1 was abundantly increased in the renal tubules of MetS ($P < 0.0001$). To confirm subcellular pAKT1 localization in renal tubules, pAKT1 was co-stained with a mitochondria marker.

Under MetS conditions, renal tubular cells exhibited distinct colocalization of pAKT1 and mitochondria (Figure 5c). These results collectively indicated that MetS induced mitochondrial AKT1 signaling by phosphorylation and translocation of AKT1 into mitochondria in the renal tubules.

To further validate these findings, experiments were conducted using an additional diabetic model (DB/DB mice), which exhibits features of MetS such as obesity, insulin resistance, and hyperglycemia. Consistent with the observations in the HFD-fed C57BL/6 model, DB/DB mice displayed significant renal damage, characterized by prominent glomerular injury, tubular swelling, and disrupted architecture (Supplementary Figure S2), along with significantly increased activation of mitochondrial pAKT1 in renal tubules compared with WT controls. Immunohistochemical staining demonstrated minimal pAKT1 expression in the renal tubules of WT mice, mild increases in DB/WT mice, and a marked elevation in DB/DB mice, particularly in the cortical and medullary tubular regions (Supplementary Figure S3).

These results were further supported by immunofluorescence co-staining of pAKT1 and mitochondria, which revealed robust colocalization of pAKT1 with mitochondria in the renal tubular cells of DB/DB mice (Supplementary Figure S4), consistent with the findings in MetS (Figure 5c). Together, these findings collectively indicate that MetS induces mitochondrial AKT1 signaling by phosphorylation and translocation of AKT1 into mitochondria in renal tubules.

Inhibition of Renal Tubule Mitochondrial AKT Signaling Aggravated MetS Renal Injuries *In Vitro*

To test the hypothesis that mitochondrial AKT1 played a protective role in renal injury induced by MetS, the MetS renal injury was induced with HK2 cells treated with palmitic acid *in vitro*. To verify the effect of MetS on renal tubular cells and whether there was a dose and time effect, HK2 cells were treated with 50 μM, 100 μM, and 200 μM palmitic acid. Upon palmitic acid treatment, there were no significant differences in the viability of HK2 cells (Figure 6a). However, a notable decrease in HK2 cell viability occurred 48 hours after heat shock protein 90 inhibitors (1 μM PU-H71 or 100 nM alvespimycin hydrochloride) treatment (decrease 56.2%, decrease 32.2%, separately at 48 h) compared with the vehicle-treated control group. These results highlight the protective role of mitochondrial AKT1 in maintaining renal tubular cell integrity under MetS conditions. Blocking the translocation of AKT1 into mitochondria exacerbated renal injury, further implicating mitochondrial AKT1 signaling in renal protection (Figure 7).

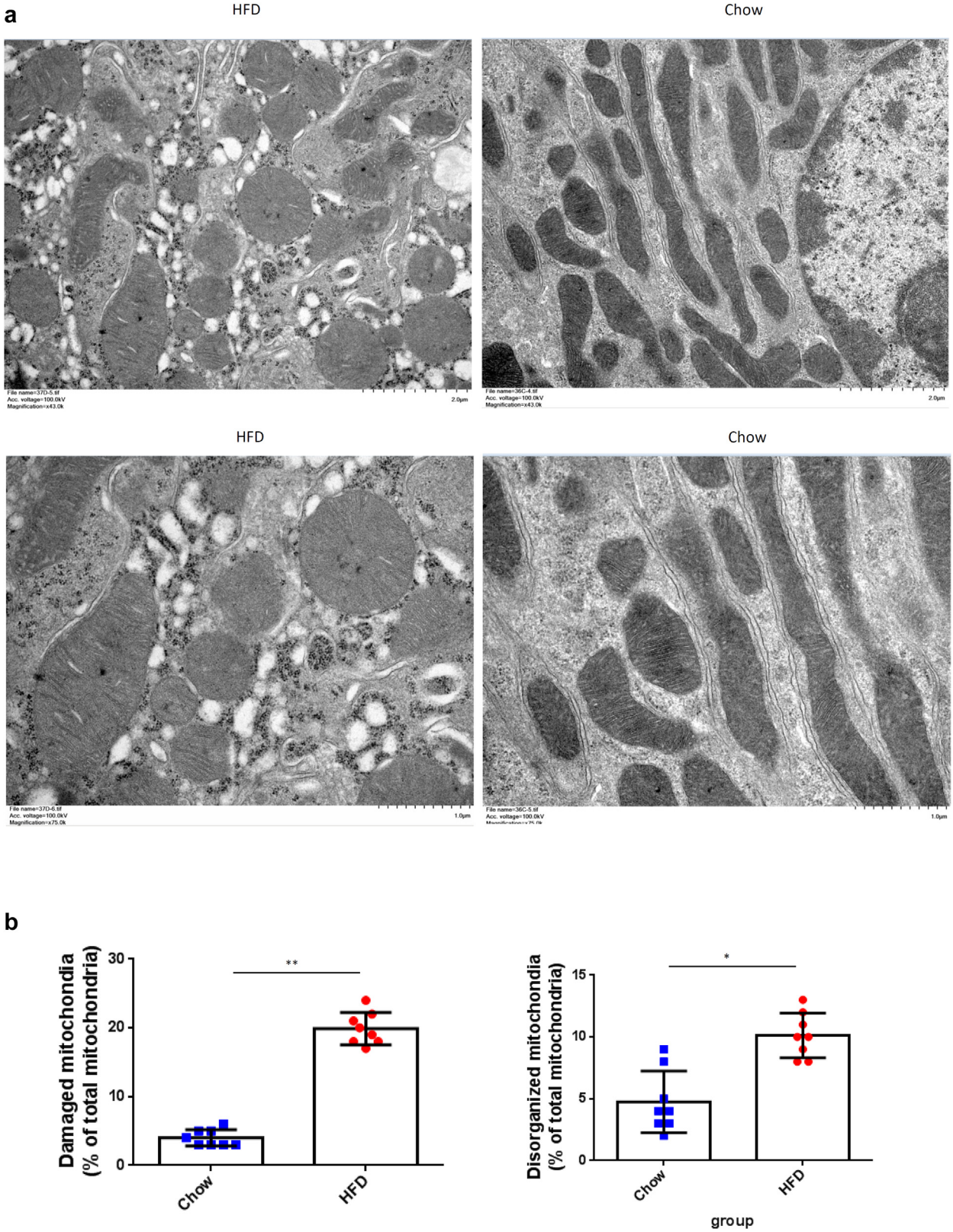

Figure 4. Metabolic syndrome altered the mitochondrial ultrastructure of renal tubular cells. The transmission electron microscope was used to investigate the effect of mitochondrial ultrastructure of metabolic syndrome on renal tubular cells. (a) HFD mice exhibited more aberrant mitochondria with hyperlucency, loss of cristae, loss of electron-dense mitochondrial matrix, and loss or disruption of the outer membranes in renal tubular cells compared with the control group. (b) Morphometric analysis revealed a significantly higher aberrant mitochondrial area ratio ($P < 0.0001$). (c) In HFD, a significant decrease in the total cristae length of the mitochondrial area was observed compared with the standard chow diet group ($P = 0.0012$). (d) The cristae number per mitochondrial area was significantly reduced area in HFD, compared with the standard chow diet group) ($P < 0.0001$). HFD, high-fat diet.

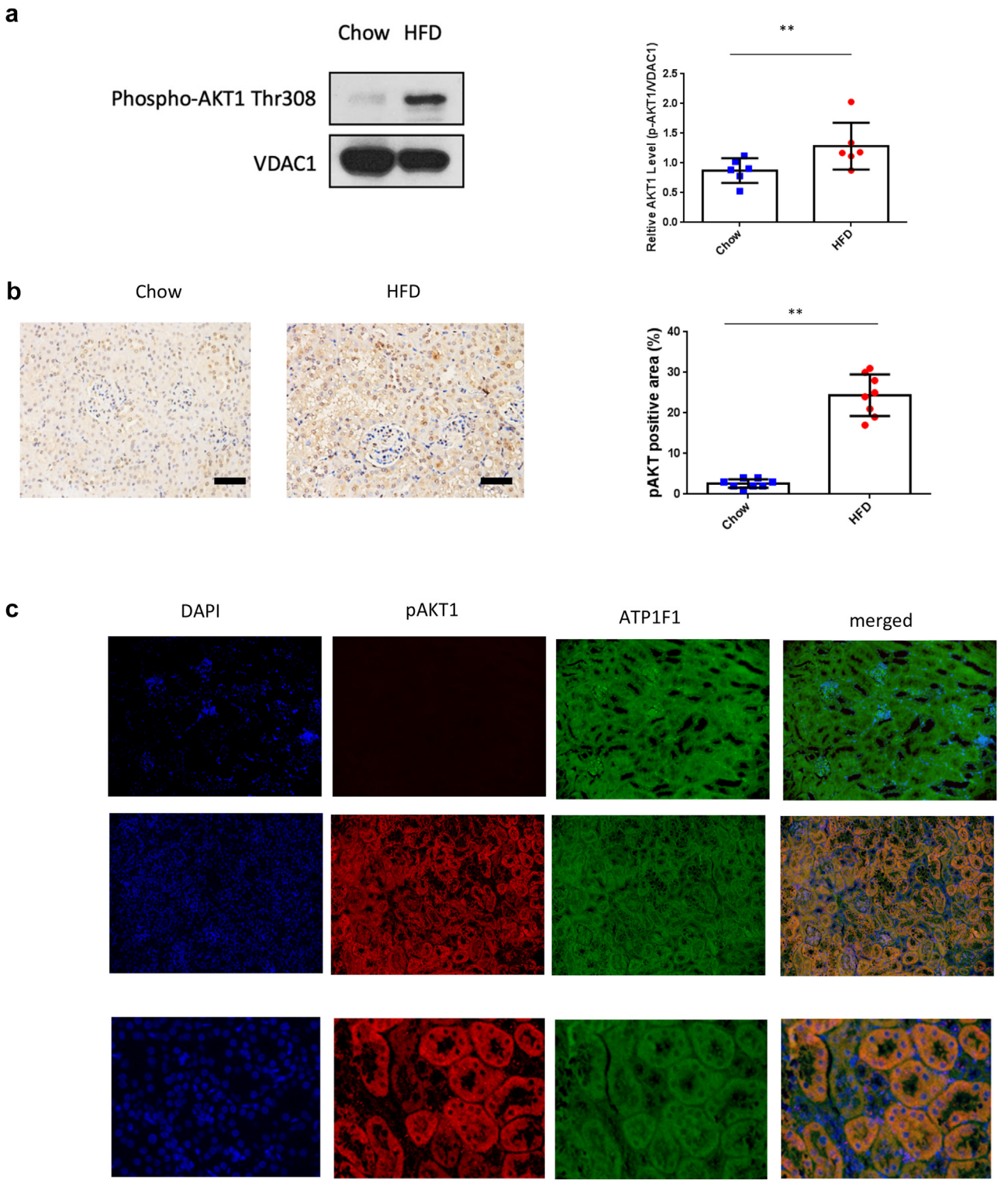

Figure 5. Activation and translocation of renal tubular mitochondrial AKT1 in metabolic syndrome. Mitochondrial fractions were isolated by gradient centrifugation of kidneys harvested from mice after 16 weeks. Western blotting analyzed protein lysate with antibodies for pAKT1, mitochondria marker VDAC. (a) The content of pAKT1 protein in mitochondria was increased in HFD mice ($P = 0.0474$). (b) Renal sections from the control or HFD were used to visualize AKT1 phosphorylation in tubules with immunohistochemistry staining. A histogram shows increased pAKT-positive areas (%) ($P < 0.0001$, $n = 6$ in each group). (c) To further characterize the colocalization of pAKT1 with tubule mitochondria, renal sections were stained with pAKT1 antibodies and ATP1F1. There was a distinct colocalization of pAKT1 and mitochondria in the renal tubules after HFD for 16 weeks. HFD, high-fat diet.

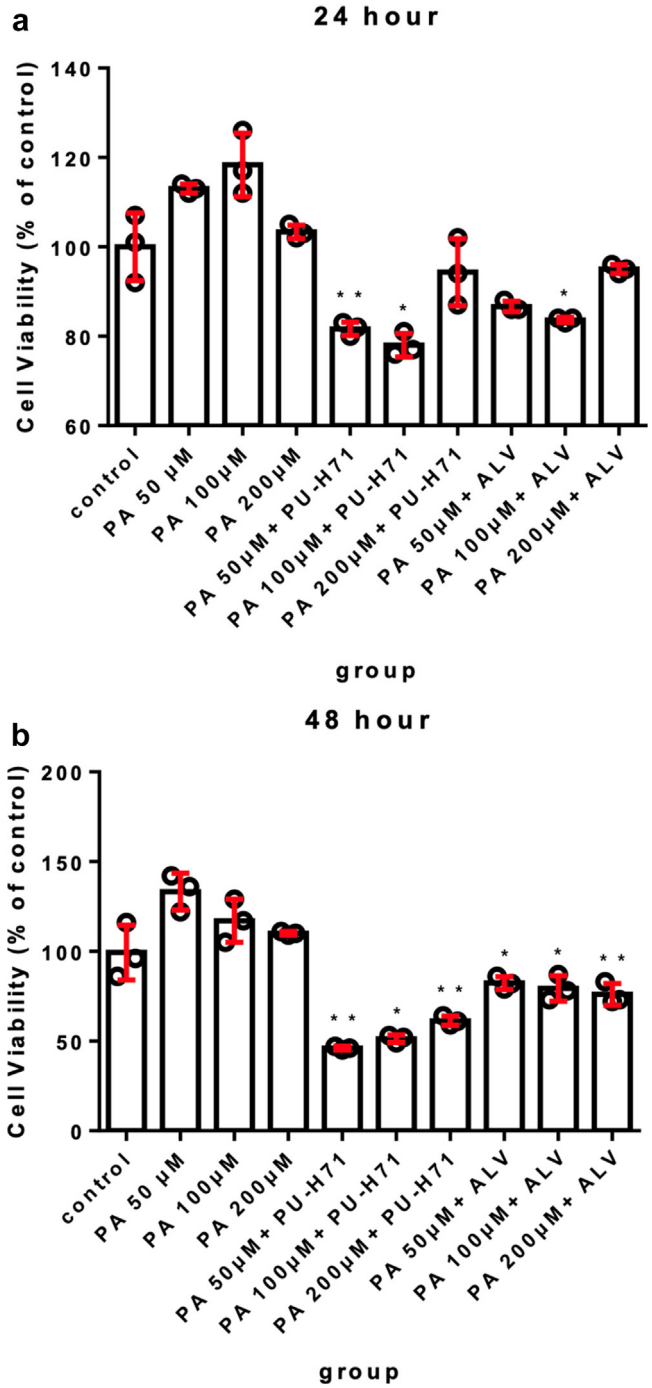

Figure 6. Inhibition of the translocation of mitochondrial AKT1 aggravates metabolic syndrome–related renal injuries. Cell viability in HK2 cells was assessed using the CCK-8 assay after treatment with various concentrations of palmitic acid alone (50, 100, 200 μM) or in combination with heat shock protein 90 (HSP90) inhibitors (1 μM PU-H71 or 100 nM alvespimycin hydrochloride). The cells were collected at 48 hours for analysis. The CCK-8 cell viability assay was conducted on HK-2 cells (a) posttreatment. Statistical significance is indicated by $^{*}P < 0.05$; $^{**}P < 0.01$. ALV, alvespimycin hydrochloride; CN, control; PA, palmitic acid.

DISCUSSION

This study elucidated the role of MetS in inducing the translocation of activated AKT1 to mitochondria in proximal renal tubules. Mice with MetS exhibited significant weight gain, impaired glucose handling, and decreased energy expenditure. The MetS-related kidney injuries were confirmed with markers of renal damage and histological analysis. Transmission electron microscopy analysis revealed an increased prevalence of aberrant mitochondria and a reduction in both cristae length and cristae density. Furthermore, pAKT1 accumulated in the mitochondria of renal tubules. These findings suggest that mitochondrial AKT1 activation serves as a protective mechanism in response to MetS, with its inhibition exacerbating renal tubular cell injuries. Thus, mitochondrial AKT1 signaling in renal tubules is pivotal in the progression of kidney failure associated with MetS.

MetS-Related Kidney Diseases

The risk of chronic kidney disease in patients with MetS increases annually with the age of onset of the disease. Through regression analysis, it has been confirmed that the risk of chronic kidney disease is independent of traditional risk factors for kidney diseases, such as hypertension, diabetes mellitus, and dyslipidemia.[20,21] Although the exact mechanisms by which MetS leads to kidney disease have not been fully elucidated, insulin resistance has been identified as the central pathogenic mechanism of MetS and its associated renal disease.[22] The atherosclerosis risk in communities study identified insulin resistance as an independent and significant factor in the development of chronic kidney disease in humans.[23] The prevention of renal and vascular end-stage disease study, demonstrated that higher fasting insulin levels were associated with age-related decline in renal function in a parabolic shape.[24] As demonstrated in this study, glucose handling was impaired in HFD-induced MetS. In addition, insulin resistance was significantly elevated in the MetS group. Furthermore, MetS decreased the respiratory exchange rate and thermogenesis.

The Character of Renal Proximal Tubular Cells of MetS-Related Kidney Injuries

Research by D'Agati has shown that the renal pathology of MetS ranges from focal segmental glomerulosclerosis to overall glomerular hypertrophy and podocyte hyperplasia, along with matrix accumulation and a reduction in normal podocyte density.[25] We also observed similar glomerular changes in our MetS rodent models (Figure 3g). The primary mechanisms by which MetS impacts the kidney include glomerular hyperfiltration, endothelial dysfunction, and glomerular hypertension, often driven by hyperinsulinemia.[26,27] Hyperfiltration results from increased renal plasma flow and heightened filtration fraction, frequently

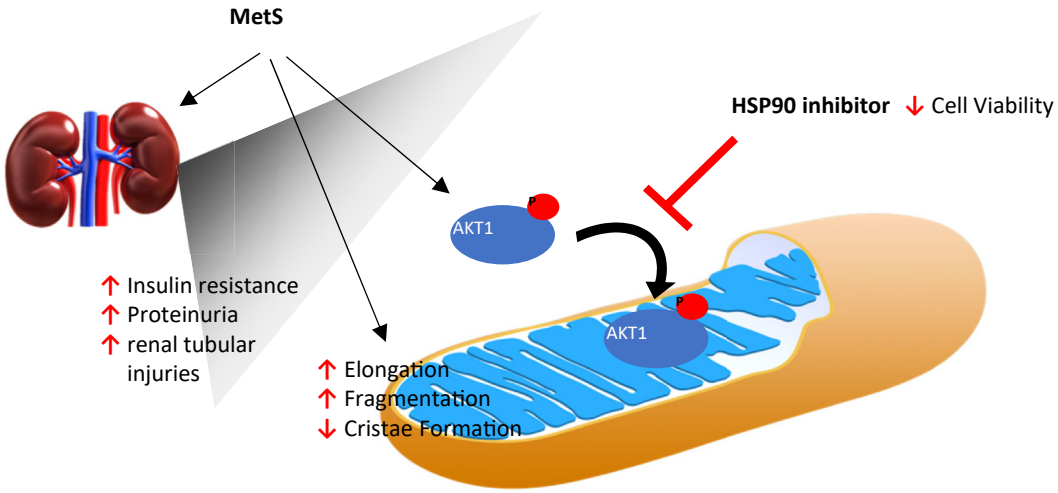

Figure 7. The role of tubular mitochondrial AKT1 in MetS. In the schematic diagram of the role of mitochondrial AKT1 in MetS-related kidney injuries, MetS increases insulin resistance, proteinuria, and renal tubular injuries. There are increasing aberrant mitochondria, decreased cristae length, and cristae numbers of MetS-related kidney injuries. Inhibition of the translocation of mitochondrial AKT1 aggravated renal tubular injuries. MetS, metabolic syndrome.

observed in the early stages of MetS. Endothelial dysfunction caused by chronic oxidative stress and systemic inflammation disrupts the glomerular filtration barrier, allowing proteinuria to develop.[28] Moreover, glomerular hypertension because of systemic hyperinsulinemia and sodium retention further exacerbates glomerular injury.[29] These glomerular changes contribute to the characteristic hypertrophy and sclerosis associated with MetS-related nephropathy.

However, the interstitium, though traditionally thought to be secondarily affected because of glomerular damage, is increasingly recognized as an independent target of injury in MetS.[30] Chronic metabolic stressors such as hyperglycemia, insulin resistance, and dyslipidemia directly impair tubular and interstitial function. Tubular injury, driven by mitochondrial dysfunction, leads to adenosine triphosphate (ATP) depletion, reactive oxygen species (ROS) generation, and subsequent oxidative damage.[31] These mitochondrial defects also contribute to inflammation, fibrosis, and eventual interstitial damage, which can occur independently or in parallel with glomerular injury.

In MetS-related kidney injuries, subsequent studies have found that in addition to the known glomerular changes, proximal tubular cells have also been found to play an important role. The study by Tobar *et al*. found that the proximal tubular epithelial cells in MetS nephropathy are hypertrophied and thickened.[32] Owing to their physiological functions, proximal renal tubular cells play an important role in renal hemodynamics and metabolic management. As MetS progresses, proximal tubular cells will compensatorily increase sodium and albumin reabsorption through the mTOR signaling pathway.[32] The PI3K/AKT/mTOR signaling pathway is crucial in maintaining cellular homeostasis and responding to metabolic stress.[33] When proteinuria occurs in the urine, the endocytic uptake of albumin by renal tubular cells activates phosphatidylinositol 3-kinase to regulate mTOR signaling.[34] mTOR plays an important role in signal regulation. It not only has a significant regulatory role in cell growth and apoptosis but is also a key regulatory protein of mitochondrial metabolism.[35] Our study results align with previous research, demonstrating not only glomerulopathy but also renal tubular injuries, particularly alterations in renal proximal tubules, as observed in our MetS rodent models depicted in Figure 3f.

The Role of Mitochondria in MetS-Related Kidney Injuries

The kidney is one of the most energy-demanding organs in the human body.[36] Nutrient-sensing pathways directly influence mitochondrial energy production when exposed to external stress stimuli such as oxidative stress, hypoxia, or energy deficiency. Alterations or reductions in ATP production, coupled with mitochondrial dysfunction, lead to the generation of high levels of ROS, disrupting the homeostasis of kidney cells. ROS can activate various cell death pathways, including apoptosis, necrosis, and autophagy. ROS promote the release of cytochrome C from mitochondria, triggering the activation of caspases and the apoptotic signaling cascade.[37] Both proximal and distal tubular cells of the kidney are essential for their reabsorption functions and their role in gluconeogenesis under conditions such as starvation, metabolic acidosis, steroid treatment, and elevated catecholamine levels.[38] The majority of renal mitochondria reside in

the proximal tubules. A mitochondrion serves as a significant cellular organelle that metabolizes nutrients for ATP production. In MetS, mitochondrial dysfunction is implicated in the pathogenesis of oxidative stress and systemic.[39] Our findings indicate that mitochondrial dysfunction is evident in renal proximal tubules affected by MetS-related kidney injuries.

Whereas our study focuses on mitochondrial dysfunction in MetS-related kidney injuries, similar mechanisms are observed in other forms of tubular injury, including ischemia-reperfusion injury and nephrotoxic drug-induced AKI. Mitochondrial dysfunction is a shared driver of these pathologies, characterized by ATP depletion, excessive ROS production, and impaired oxidative phosphorylation. For example, our previous study demonstrated that tubular mitochondrial AKT1 activation occurs during ischemia-reperfusion injury, contributing to chronic kidney disease progression.[15] In addition, we have shown that mitochondrial ATP synthase dysfunction plays a critical role in maleic acid–induced AKI, resulting in energy depletion and tubular cell apoptosis.[16]

Mitochondrial AKT1 regulates cellular oxidative phosphorylation, ROS, and cell survival.[40] Impaired mitochondrial AKT1 signaling uncoupled respiration and lowered ATP production, as shown in our previous study.[15] Although renal tubular apoptosis is a common finding in various models of renal injuries, the signaling pathways upstream from mitochondria were not entirely clear.[41] The apoptosis and subsequent loss of tubular cells have been identified as pivotal factors in the progression of renal injuries.[42] Moreover, tubular repair and regeneration is proposed as a significant event in the recovery from such injuries.[18,19,43,44] Although sublethal injuries may potentially be reversible, the death of tubular cells invariably results in the permanent loss of tubular function.[45] The loss of mitochondrial cross-membrane electrochemical gradient is a critical checkpoint that initiates apoptosis.[46] Mitochondrial leakage, regulated by mitochondrial AKT1, likely represents a decisive juncture in the determination between cell survival and apoptotic cell death.[47,48] Our study results offer new insights into the role of mitochondria in mitigating kidney injury associated with MetS. Inhibition of mitochondrial AKT1 during MetS resulted in eventual tubular cell death (Figure 6).

Limitations

MetS is a multifaceted condition encompassing a diverse range of pathophysiological processes. These complexities make it challenging for any single animal model to fully recapitulate all aspects of MetS and its associated complications. We employed the HFD-fed C57BL/6 mouse model, a widely used and well-established model to induce features of MetS, such as obesity, glucose dysregulation, and insulin resistance. To address this limitation, we conducted complementary experiments using DB/DB mice, a genetic model of diabetes and obesity, to validate our findings. Future studies could incorporate additional MetS-mimicking models to capture the broader spectrum of renal injury mechanisms associated with MetS.

CONCLUSION

Our study addresses a significant knowledge gap about the involvement of proximal renal tubule mitochondria in MetS-related kidney injuries through the activation and translocation of AKT1 into mitochondria. This mechanism of renal protection suggests a novel target for developing strategies to improve the prevention and treatment of acute and chronic kidney injuries. Future research should explore new approaches to enhance AKT1 activity in proximal tubule mitochondria to prevent MetS-related kidney injuries better.

DISCLOSURE

All the authors declared no conflicting interests.

ACKNOWLEDGMENTS

The authors thank the Center for Laboratory Animals in Kaohsiung Medical University for animal care. The transmission electron microscopy examination was supported by Microscope Core Laboratory, Chang Gung Memorial Hospital, Linkou. We sincerely thank Dr. Yen-Yi Zhen and Dr. Chao-Hung Chen for their invaluable contributions in conducting the DB/DB mouse experiments, which significantly enhanced the scope and robustness of this study.

Funding

Funding was provided by the Ministry of Science and Technology (110-2314-B-037-068-MY3, 113-2314-B-037-107-MY3), Kaohsiung Medical University (NK113P22, NK114P_14, KMTTH-DK(A)114001), and Chang Gung Memorial Hospital (CMRPD8J0011, CMRPD8J0012, CMRPD8J0013, and CMRPD8P0011). The findings and conclusions in this report are those of the authors and do not necessarily represent the official position of the funding organizations.

AUTHOR CONTRIBUTIONS

HL and MY conceived the project and designed the experiments. YC, TW, and CY executed the experiments. YC and YHC contributed to data interpretation and modification of experiment design. The manuscript was composed by HL, with input from all the authors. Statistical analyses were performed by HL, YC, and TW. DFD, JF, and YC provided overall supervision of the project.

SUPPLEMENTARY MATERIAL

Supplementary File (PDF)

Figure S1. Baseline characteristics of high-fat diet and standard chow diet groups

Figure S2. Histological analysis of renal tissue in WT, DB/WT, and DB/DB mice.

Figure S3. Immunohistochemical staining for pAKT1 in renal tissue of WT, DB/WT, and DB/DB mice.

Figure S4. Immunofluorescence staining for pAKT1 and mitochondrial markers in renal tubules of WT and DB/DB mice.

REFERENCES

1. Alberti KG, Eckel RH, Grundy SM, et al. Harmonizing the metabolic syndrome: a joint interim statement of the International Diabetes Federation Task Force on Epidemiology and Prevention; National Heart, Lung, and Blood Institute; American Heart Association; World Heart Federation; International Atherosclerosis Society; and International Association for the Study of Obesity. *Circulation*. 2009;120:1640–1645. https://doi.org/10.1161/CIRCULATIONAHA.109.192644
2. Noubiap JJ, Nansseu JR, Lontchi-Yimagou E, et al. Global, regional, and country estimates of metabolic syndrome burden in children and adolescents in 2020: a systematic review and modelling analysis. *Lancet Child Adolesc Health*. 2022;6:158–170. https://doi.org/10.1016/S2352-4642(21)00374-6
3. Locatelli F, Pozzoni P, Del Vecchio L. Renal manifestations in the metabolic syndrome. *J Am Soc Nephrol*. 2006;17(suppl 2):S81–S85. https://doi.org/10.1681/ASN.2005121332
4. Chen J, Muntner P, Hamm LL, et al. The metabolic syndrome and chronic kidney disease in U.S. adults. *Ann Intern Med*. 2004;140:167–174. https://doi.org/10.7326/0003-4819-140-3-200402030-00007
5. Lin HY, Chang LY, Niu SW, et al. High risk of renal outcome of metabolic syndrome independent of diabetes in patients with CKD stage 1–4: the ICKD database. *Diabetes Metab Res Rev*. 2023;39:e3618. https://doi.org/10.1002/dmrr.3618
6. Shen FC, Lin HY, Tsai WC, et al. Non-insulin-based insulin resistance indices for predicting all-cause mortality and renal outcomes in patients with stage 1–4 chronic kidney disease: another paradox. *Front Nutr*. 2023;10:1136284. https://doi.org/10.3389/fnut.2023.1136284
7. Hung CC, Zhen YY, Niu SW, et al. Predictive value of HbA1c and metabolic syndrome for renal outcome in non-diabetic CKD Stage 1–4 patients. *Biomedicines*. 2022;10:1858. https://doi.org/10.3390/biomedicines10081858
8. Schneeberger M, Dietrich MO, Sebastian D, et al. Mitofusin 2 in POMC neurons connects ER stress with leptin resistance and energy imbalance. *Cell*. 2013;155:172–187. https://doi.org/10.1016/j.cell.2013.09.003
9. Szendroedi J, Phielix E, Roden M. The role of mitochondria in insulin resistance and type 2 diabetes mellitus. *Nat Rev Endocrinol*. 2011;8:92–103. https://doi.org/10.1038/nrendo.2011.138
10. Gai Z, Wang T, Visentin M, Kullak-Ublick GA, Fu X, Wang Z. Lipid accumulation and chronic kidney disease. *Nutrients*. 2019;11:722. https://doi.org/10.3390/nu11040722
11. Ruggiero C, Ehrenshaft M, Cleland E, Stadler K. High-fat diet induces an initial adaptation of mitochondrial bioenergetics in the kidney despite evident oxidative stress and mitochondrial ROS production. *Am J Physiol Endocrinol Metab*. 2011;300:E1047–E1058. https://doi.org/10.1152/ajpendo.00666.2010
12. Hemmings BA, Restuccia DF. The PI3K-PKB/Akt pathway. *Cold Spring Harb Perspect Biol*. 2015;7:a026609. https://doi.org/10.1101/cshperspect.a026609
13. Wang H, Ai J, Shopit A, et al. Protection of pancreatic β-cell by phosphocreatine through mitochondrial improvement via the regulation of dual AKT/IRS-1/GSK-3β and STAT3/Cyp-D signaling pathways. *Cell Biol Toxicol*. 2022;38:531–551. https://doi.org/10.1007/s10565-021-09644-7
14. Ali MZ, Dholaniya PS. Oxidative phosphorylation mediated pathogenesis of Parkinson's disease and its implication via Akt signaling. *Neurochem Int*. 2022;157:105344. https://doi.org/10.1016/j.neuint.2022.105344
15. Lin HY, Chen Y, Chen YH, et al. Tubular mitochondrial AKT1 is activated during ischemia reperfusion injury and has a critical role in predisposition to chronic kidney disease. *Kidney Int*. 2021;99:870–884. https://doi.org/10.1016/j.kint.2020.10.038
16. Lin HY, Liang CJ, Yang MY, et al. Critical roles of tubular mitochondrial ATP synthase dysfunction in maleic acid-induced acute kidney injury. *Apoptosis*. 2024;29:620–634. https://doi.org/10.1007/s10495-023-01897-3
17. McAllan L, Skuse P, Cotter PD, et al. Protein quality and the protein to carbohydrate ratio within a high fat diet influences energy balance and the gut microbiota in C57BL/6J mice. *PLoS One*. 2014;9:e88904. https://doi.org/10.1371/journal.pone.0088904
18. Sharfuddin AA, Molitoris BA. Pathophysiology of ischemic acute kidney injury. *Nat Rev Nephrol*. 2011;7:189–200. https://doi.org/10.1038/nrneph.2011.16
19. Zarjou A, Agarwal A. Sepsis and acute kidney injury. *J Am Soc Nephrol*. 2011;22:999–1006. https://doi.org/10.1681/ASN.2010050484
20. Hsu CY, McCulloch CE, Iribarren C, Darbinian J, Go AS. Body mass index and risk for end-stage renal disease. *Ann Intern Med*. 2006;144:21–28. https://doi.org/10.7326/0003-4819-144-1-200601030-00006
21. Tan CE, Ma S, Wai D, Chew SK, Tai ES. Can we apply the National Cholesterol Education Program Adult Treatment Panel definition of the metabolic syndrome to Asians? *Diabetes Care*. 2004;27:1182–1186. https://doi.org/10.2337/diacare.27.5.1182
22. Reaven GM. Role of insulin resistance in human disease (syndrome X): an expanded definition. *Annu Rev Med*. 1993;44:121–131. https://doi.org/10.1146/annurev.me.44.020193.001005
23. Folsom AR, Eckfeldt JH, Weitzman S, et al. Relation of carotid artery wall thickness to diabetes mellitus, fasting glucose and insulin, body size, and physical activity. Atherosclerosis Risk in Communities (ARIC) study investigators. *Stroke*. 1994;25:66–73. https://doi.org/10.1161/01.str.25.1.66
24. Kurella M, Lo JC, Chertow GM. Metabolic syndrome and the risk for chronic kidney disease among nondiabetic adults. *J Am Soc Nephrol*. 2005;16:2134–2140. https://doi.org/10.1681/ASN.2005010106

25. Kambham N, Markowitz GS, Valeri AM, Lin J, D'Agati VD. Obesity-related glomerulopathy: an emerging epidemic. *Kidney Int*. 2001;59:1498–1509. https://doi.org/10.1046/j.1523-1755.2001.0590041498.x
26. de Jong PE, Verhave JC, Pinto-Sietsma SJ, Hillege HL, PREVEND study group. Obesity and target organ damage: the kidney. *Int J Obes Relat Metab Disord*. 2002;26(suppl 4):S21–S24. https://doi.org/10.1038/sj.ijo.0802213
27. Forbes JM, Thorburn DR. Mitochondrial dysfunction in diabetic kidney disease. *Nat Rev Nephrol*. 2018;14:291–312. https://doi.org/10.1038/nrneph.2018.9
28. Zhan M, Brooks C, Liu F, Sun L, Dong Z. Mitochondrial dynamics: regulatory mechanisms and emerging role in renal pathophysiology. *Kidney Int*. 2013;83:568–581. https://doi.org/10.1038/ki.2012.441
29. Hostetter TH. Hyperfiltration and glomerulosclerosis. *Semin Nephrol*. 2003;23:194–199. https://doi.org/10.1053/anep.2003.50017
30. Decleves AE, Sharma K. Obesity and kidney disease: differential effects of obesity on adipose tissue and kidney inflammation and fibrosis. *Curr Opin Nephrol Hypertens*. 2015;24:28–36. https://doi.org/10.1097/MNH.0000000000000087
31. Hall ME, do Carmo JM, da Silva AA, Juncos LA, Wang Z, Hall JE. Obesity, hypertension, and chronic kidney disease. *Int J Nephrol Renovasc Dis*. 2014;7:75–88. https://doi.org/10.2147/IJNRD.S39739
32. Tobar A, Ori Y, Benchetrit S, et al. Proximal tubular hypertrophy and enlarged glomerular and proximal tubular urinary space in obese subjects with proteinuria. *PLoS One*. 2013;8:e75547. https://doi.org/10.1371/journal.pone.0075547
33. Wang H, Gao L, Zhao C, et al. The role of PI3K/Akt signaling pathway in chronic kidney disease. *Int Urol Nephrol*. 2024;56:2623–2633. https://doi.org/10.1007/s11255-024-03989-8
34. Brunskill NJ, Stuart J, Tobin AB, Walls J, Nahorski S. Receptor-mediated endocytosis of albumin by kidney proximal tubule cells is regulated by phosphatidylinositide 3-kinase. *J Clin Invest*. 1998;101:2140–2150. https://doi.org/10.1172/JCI1923
35. Ramanathan A, Schreiber SL. Direct control of mitochondrial function by mTOR. *Proc Natl Acad Sci U S A*. 2009;106:22229–22232. https://doi.org/10.1073/pnas.0912074106
36. Wang Z, Ying Z, Bosy-Westphal A, et al. Specific metabolic rates of major organs and tissues across adulthood: evaluation by mechanistic model of resting energy expenditure. *Am J Clin Nutr*. 2010;92:1369–1377. https://doi.org/10.3945/ajcn.2010.29885
37. Mahmoodnia L, Aghadavod E, Beigrezaei S, Rafieian-Kopaei M. An update on diabetic kidney disease, oxidative stress and antioxidant agents. *J Ren Inj Prev*. 2017;6:153–157. https://doi.org/10.15171/jrip.2017.30
38. Schoolwerth AC, Smith BC, Culpepper RM. Renal gluconeogenesis. *Miner Electrolyte Metab*. 1988;14:347–361.
39. Prasun P. Mitochondrial dysfunction in metabolic syndrome. *Biochim Biophys Acta Mol Basis Dis*. 2020;1866:165838. https://doi.org/10.1016/j.bbadis.2020.165838
40. Su CC, Yang JY, Leu HB, Chen Y, Wang PH. Mitochondrial Akt-regulated mitochondrial apoptosis signaling in cardiac muscle cells. *Am J Physiol Heart Circ Physiol*. 2012;302:H716–H723. https://doi.org/10.1152/ajpheart.00455.2011
41. Gewin LS. Sugar or fat? Renal tubular metabolism reviewed in health and disease. *Nutrients*. 2021;13:1580. https://doi.org/10.3390/nu13051580
42. Wang Y, Jin M, Cheng CK, Li Q. Tubular injury in diabetic kidney disease: molecular mechanisms and potential therapeutic perspectives. *Front Endocrinol (Lausanne)*. 2023;14:1238927. https://doi.org/10.3389/fendo.2023.1238927
43. Bonventre JV, Yang L. Cellular pathophysiology of ischemic acute kidney injury. *J Clin Invest*. 2011;121:4210–4221. https://doi.org/10.1172/JCI45161
44. Kinsey GR, Sharma R, Okusa MD. Regulatory T cells in AKI. *J Am Soc Nephrol*. 2013;24:1720–1726. https://doi.org/10.1681/ASN.2013050502
45. Ratliff BB, Rabadi MM, Vasko R, Yasuda K, Goligorsky MS. Messengers without borders: mediators of systemic inflammatory response in AKI. *J Am Soc Nephrol*. 2013;24:529–536. https://doi.org/10.1681/ASN.2012060633
46. Martinou JC, Green DR. Breaking the mitochondrial barrier. *Nat Rev Mol Cell Biol*. 2001;2:63–67. https://doi.org/10.1038/35048069
47. Green DR, Ferguson T, Zitvogel L, Kroemer G. Immunogenic and tolerogenic cell death. *Nat Rev Immunol*. 2009;9:353–363. https://doi.org/10.1038/nri2545
48. Kroemer G, Galluzzi L, Brenner C. Mitochondrial membrane permeabilization in cell death. *Physiol Rev*. 2007;87:99–163. https://doi.org/10.1152/physrev.00013.2006